Chemical Imaging of Poplar Wood Cell Walls by Confocal Raman Microscopy

Notburga Gierlinger* and Manfred Schwanninger

Max-Planck-Institute of Colloids and Interfaces, Department of Biomaterials, 14424 Potsdam, Germany (N.G.); and BOKU-University of Natural Resources and Applied Life Sciences, Department of Chemistry, 1190 Vienna, Austria (M.S.)

Confocal Raman microscopy was used to illustrate changes of molecular composition in secondary plant cell wall tissues of poplar (*Populus nigra* × *Populus deltoids*) wood. Two-dimensional spectral maps were acquired and chemical images calculated by integrating the intensity of characteristic spectral bands. This enabled direct visualization of the spatial variation of the lignin content without any chemical treatment or staining of the cell wall. A small (0.5 μm) lignified border toward the lumen was observed in the gelatinous layer of poplar tension wood. The variable orientation of the cellulose was also characterized, leading to visualization of the S1 layer with dimensions smaller than 0.5 μm. Scanning Raman microscopy was thus shown to be a powerful, nondestructive tool for imaging changes in molecular cell wall organization with high spatial resolution.

The plant cell wall in wood tissue has a multicomposite structure, consisting of several layers formed at different periods during cell differentiation. After the cell wall reaches its final size, the mechanically crucial secondary cell wall, consisting of three different sublayers (S1, S2, and S3) is formed (Plomion et al., 2001). The cellulose microfibril orientation and chemical composition varies between the sublayers. The S2 layer is the thickest (75%–85% of the total thickness of the cell wall) and most important for mechanical stability (Fengel and Wegener, 1989). Between adjacent cells, a middle lamella layer attached to the primary cell wall ensures the adhesion of a cell to its neighbors. The chemical composition of the cell wall and the alignment of the cellulose microfibrils show significant interspecies and intraspecies variability (e.g. Côté and Day, 1965; Barnett and Bonham, 2004).

As a response to a nonvertical orientation of the stem or branch, which may arise due to prevailing winds, snow, slope, or asymmetric crown shape, a specialized wood tissue called reaction wood is formed. It is usually associated with eccentric growth and changes in structure and chemistry (Côté and Day, 1965). In hardwood species the reaction wood tends to form in zones held in tension, e.g. on the upper side of a leaning stem (Barnett and Jeronimidis, 2003). These tension wood fibers are characterized by a thick cell wall and a special cell wall layer, usually referred to as the gelatinous layer (G-layer), which is not found in normal wood fibers (Côté et al., 1969). Although several theories about the generation of these growth stresses (e.g. Sugiyama et al., 1993; Yamamoto, 1998; Bamber, 2001) and knowledge about changes in anatomy, chemistry, and the microfibril angle (e.g. Côté and Day, 1965; Timell, 1969; Jourez et al., 2001) exist, a complete understanding is still lacking.

Most traditional chemical analyses of plant cell walls are destructive, since they require disintegration of the plant tissue. In addition, sample isolation difficulties arise when small cell wall areas or single layers are of interest since they have to be carefully excised. Therefore, the ability to generate images of the chemical composition from plant cell wall in situ and nondestructively (i.e. in its original anatomical context in the tissue sample) would be a significant advance. Infrared and Raman spectroscopy recently found application as chemical mapping and imaging techniques for biological and biomimetic samples (Salzer et al., 2000; Chenery and Bowring, 2003). Both methods are based on discrete vibrational transitions that take place in the ground electronic state of molecules. While Raman scattering involves excitation of a molecule by inelastic scattering with a photon (from a laser light source), infrared absorption spectroscopy typically involves photon absorption, with the molecule excited to a higher vibrational energy level (Schrader, 1995). Raman scattering depends on changes in the polarizability of functional groups due to molecular vibration, while infrared absorption depends on changes in the intrinsic dipole moments (Smith and Dent, 2005). Therefore, Raman and infrared spectroscopy can provide complementary information about the molecular vibrations. Both methods have developed as important tools in plant cell wall research (e.g. Atalla and Agarwal, 1985; McCann et al., 1992; Séné et al., 1994; Stewart, 1996; Himmelsbach et al., 1999; Kacuráková et al., 2000; McCann et al., 2001; Morris

* Corresponding author; e-mail gierlinger@mpikg.mpg.de; fax 49–331–567–9402.

The author responsible for distribution of materials integral to the findings presented in this article in accordance with the policy described in the Instructions for Authors (www.plantphysiol.org) is: Notburga Gierlinger (gierlinger@mpikg.mpg.de).

Article, publication date, and citation information can be found at www.plantphysiol.org/cgi/doi/10.1104/pp.105.066993.

et al., 2003; Toole et al., 2004), as they allow the acquisition of information concerning the molecular structure and composition of individual features of plant tissue in a close-to-native state. In combination with microscopy, Raman spectroscopy has the advantage that spectra can be acquired on aqueous, thicker (not opaque) samples with a higher spatial resolution, but sample fluorescence may limit the quality of the spectra.

In this study we demonstrate the feasibility of confocal Raman microscopy for chemical imaging of poplar (*Populus nigra* × *Populus deltoids*) wood cross sections. From both normal and tension wood zones, spectra were acquired at each point on a two-dimensional defined measurement grid (scanning Raman microscopy), followed by integration over selected bands at each point. Thus, generated two-dimensional chemical composition maps enabled us to visualize the contrast between different cell wall layers due to differences in polymer composition and/or orientation. A further analysis of the full range spectra from selected areas of the chemical images revealed explanations and details about the visualized differences in molecular structure and composition between and within cell wall layers.

RESULTS AND DISCUSSION

Normal Wood

Latewood cells adjacent to ray parenchyma cells were chosen as an example for normal poplar wood. Two-dimensional chemical images were calculated by integrating over wavenumber ranges containing strong Raman bands (Fig. 1, A–D). The lignin distribution is shown by integrating over the 1,600 cm^{-1} band (1,550–1,640 cm^{-1}), dominated by the aromatic C=C vibration (Fig. 1A). The cell corner (CC) and the compound middle lamella (CML; middle lamella + adjacent primary walls) are observed to have a higher intensity and thus higher lignin concentration than the S2 layer. The C–H stretching (str.) region from 2,780 cm^{-1} to 3,060 cm^{-1} includes contributions from lignin and carbohydrates (Table I). Integrating over this range displays higher intensities within the S2 layer of the fibers (Fig. 1B), whereas the S2 layer of ray parenchyma cells, CC, and the inner part of the fibers show less intensity. Some spherical globules appear in the lumen of the ray parenchyma cells (Fig. 1B). By integrating from 1,026 cm^{-1} to 1,195 cm^{-1}, a similar picture is obtained (Fig. 1C), whereas the CCs show less intensity, concluding that contributions from lignin are minor in this wavenumber area and distribution of carbohydrates can be followed. Finally a narrow wavenumber area (1,090–1,105 cm^{-1}), including only the cellulose orientation-sensitive band at 1,096 cm^{-1} (Agarwal and Atalla, 1986) was chosen to image different orientations of the cellulose molecules (Fig. 1D). In this mode the S2 of the parenchyma ray cell (S2ray) and small layers on both sides of the CML (e.g. Fig. 1D within the rectangle) had a higher intensity. They appear as two small layers adjacent to the CML and seem to represent the S1 (Fig. 1D). Since Figure 1C also shows a high intensity in the same regions adjacent to the CML, we conclude that the broad range integration from 1,026 cm^{-1} to 1,195 cm^{-1} comprises carbohydrate concentration together with orientation changes.

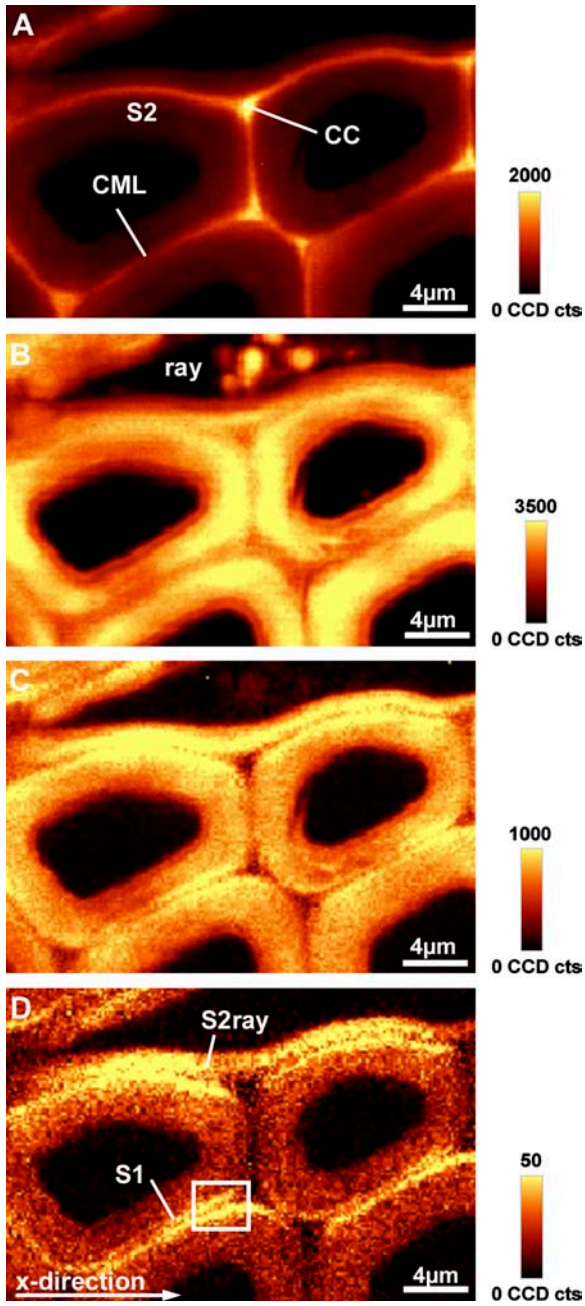

Figure 1. A to D, Raman images (30 × 20 μm) of a cross section of poplar latewood by integrating over defined wavenumber areas. A, Intensity of the aromatic lignin band (1,550–1,640 cm^{-1}). B, C–H str. region (2,780–3,060 cm^{-1}). C and D, Intensity of bands in the carbohydrate region from 1,026 to 1,195 cm^{-1} (C) and intensity of the 1,096 cm^{-1} band (1,090–1,105 cm^{-1}; D).

Table I. *The Raman bands used for analysis and their assignment to lignin (L) and/or carbohydrate components (cellulose [C], glucomannan [GlcMan], and xylan [Xyl]) according to the literature (Wiley and Atalla, 1987; Agarwal and Ralph, 1997; Edwards et al., 1997; Agarwal, 1999; Saariaho et al., 2003)*

Wavenumber	Component	Assignment
cm^{-1}		
2,945	L, GlcMan, and C	CH str. in OCH_3 asym.
2,897	C	CH and CH_2 str.
1,660	L	Ring conjugated C=C str. of coniferyl alcohol; C=O str. of coniferaldehyde
1,620	L	Ring conjugated C=C str. of coniferaldehyde
1,601	L	Aryl ring str., sym.
1,508	L	Aryl ring str., asym.
1,462	L and C	HCH and HOC bending
1,423	L	O–CH_3 deformation; CH_2 scissoring; guaiacyl ring vibration
1,376	C	HCC, HCO, and HOC bending
1,333	C	HCC and HCO bending
1,274	L	Aryl–O of aryl OH and aryl O–CH_3; guaiacyl ring (with C=O group) mode
1,150	C	Heavy atom (CC and CO) str. plus HCC and HCO bending
1,143	L ?	
1,122	C, Xyl, and GlcMan	Heavy atom (CC and CO) str.
1,096	C, Xyl, and GlcMan	Heavy atom (CC and CO) str.
1,045	L ?	CO of aryl–O–CH_3 and aryl–OH at 1,033 ?
997	C	
903	C	Heavy atom (CC and CO) str.

Average spectra were calculated for the different cell wall layers (CC, CML, S2, S2ray, and S1) and ray components (ray) by marking the distinct areas on the chemical images (Fig. 1, A–D). The spectrum of the ray components (ray) differs clearly from the cell wall spectra (Fig. 2, A and B). Strong bands are observed around 2,900 cm^{-1}, which can be assigned to the str. of C–H and C–H_2 groups, which give also rise to bands at 1,442 cm^{-1} (C–H_2 scissor deformation) and 1,303 cm^{-1} (C–H_2 twisting deformation). A band at 1,656 cm^{-1} points to an unsaturated molecule (C=C) and that at 1,740 cm^{-1} to carbonyl groups. These bands coincide with the ones described for unsaturated fatty acid esters (Rösch et al., 2004). The parenchymatous cells of wood serve as essential vegetative storage tissues in which starch, sugars, proteins, and fat accumulate seasonally. Starch accumulates from May until October, fat mainly during the summer month, and protein when the leaves are yellowing in September and October (Sauter and van Cleve, 1994). Since the poplar trees were harvested in August (summer) the presence of fatty acid esters is reasonable.

In the CML and especially the CC spectrum, a higher fluorescence background (causing a shift in the Raman intensity axis) is observed due to the higher lignin content (Fig. 2, A and B). The higher lignin content can also be seen in the strong peak at about 1,600 cm^{-1}. In the C–H str. region (2,975–2,840 cm^{-1}) of the CC spectrum, the peak at 2,945 cm^{-1} from the C–H str. of the methoxyl groups of the lignin is more pronounced, whereas in the S2 the peak at 2,897 cm^{-1}, attributed to C–H and C–H_2 str. of the cellulose, dominates (Fig. 2B; Table I). The bands at 1,122 cm^{-1} and 1,096 cm^{-1} are assigned to symmetric (sym.) and asymmetric (asym.) str. of C–O–C linkages of cellulose (Edwards et al., 1997) and are more pronounced in the CML and S2 spectra than in the CC spectrum. The lignin-rich CC shows a maximum at 1,143 cm^{-1}, which might be assigned to lignin (Fig. 2B; Table I).

The S1 spectrum was calculated by marking the visualized radial layers in Figure 1D. Higher intensities of the lignin bands are observed in the S1 spectrum compared to the S2 spectra (Fig. 2, C and D). However, due to the small dimensions of S1 and CML (Fig. 1D), we cannot interpret the higher peak as a higher lignin content in the S1 alone; probable there are contributions from the adjacent highly lignified CML. Since the three layers, S1-CML-S1, have together a width of about 0.8 μm, the displayed spectra may contain chemical information from the adjoining layer. Nevertheless, changed band height ratios of the cellulose bands in the S1 layer (Fig. 2, C and D) allowed to visualize this small layer by chemical imaging (Fig. 1D).

An even clearer change in the band height ratio of the cellulose bands is seen in the average spectrum of the S2 of the ray parenchyma cells (S2ray; Fig. 2, C and D). In the S2 of the ray cells, the band at 2,896 cm^{-1} is strongly reduced, the band at 1,096 cm^{-1} is increased, and bands at 994 cm^{-1} and 1,423 cm^{-1} appeared. These observed changes in band height ratios are in context with the orientation of the cellulose molecule: bands deriving from perpendicular oriented C–H bonds decrease (sym. str. 2,897 cm^{-1}), while the parallel oriented C–O–C (1,096 cm^{-1}) increase. These two band heights are highly sensitive to the orientation in cellulose, as well as the bands at 1,423 cm^{-1} and 994 cm^{-1} (Wiley and Atalla, 1987).

The observed differences in the S2 of ray parenchyma cells and fiber cells can be explained by the process of cell wall growth and division. The radial parenchyma cells derive from the isodiametrical ray

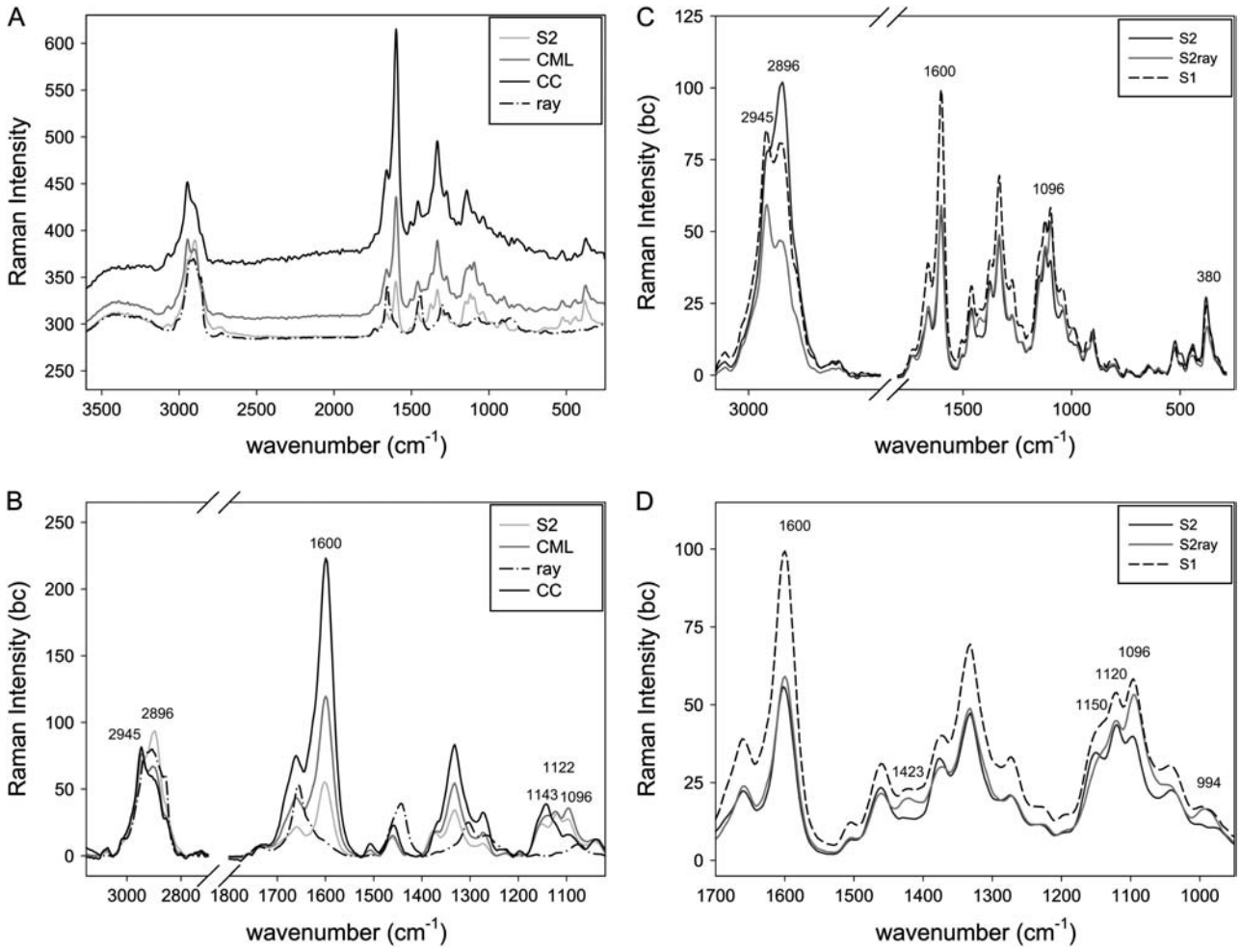

Figure 2. A to D, Average Raman spectra of the S2, CC, CML, and the ray content (ray) of poplar latewood (A), baseline corrected (bc), and zoom into the dominating bands. B, Comparison of the average bc spectra of the S2 of the fiber cells (S2), the S2 of the ray parenchyma cell (S2ray) and the S1 (C), and a zoom into the region from 950 to 1,700 cm^{-1} (D).

cambial cells by anticlinal division, whereas secondary xylem cells are added by periclinal division of an axially elongated fusiform cambial cell (Mellerowicz et al., 2001). Therefore, the ray parenchyma cell in our sample is in a plane parallel to the electric vector direction of the electromagnetic field from the laser beam, while the fiber tracheid is perpendicular. Accordingly, in the ray parenchyma cells the intensity of perpendicular oriented C–H bonds decreased (sym. str. 2,897 cm^{-1}), while the parallel oriented C–O–C bonds (1,096 cm^{-1}) increased.

In the S1 the fibrils run with a gentle helical slope (Fengel and Wegener, 1989) and are therefore more parallel to the electric vector of the laser beam in x-directions. We draw attention to the fact that such a change in the orientation-sensitive 1,096 cm^{-1} band enables us to distinguish two separate layers of only 0.3 μm thickness in a two-dimensional chemical composition image (Fig. 1D). As a technical aside, this is only visible on the radial walls in x-direction (horizontal) of the image in Figure 1D, because the laser beam is polarized in the x-direction. Turning the sample around by 90° emphasizes the S1 on the tangential walls (data not shown).

Tension Wood

Before the above investigated latewood was formed, a zone of tension wood was laid down in spring as a reaction to the tilting of the young plants. So-called G-fibers with a small S2 layer and an additional G-layer were developed. Integration over the aromatic C=C peak shows the highly lignified CCs and CML and a less-lignified small S2 layer (Fig. 3A). The G-layer, adjacent to the S2, is almost invisible, so we conclude that it is not lignified. Changing the intensity scale reveals that a small inner layer (G_{in}) contains more aromatic compounds (Fig. 3B). In some cases aromatic structures extend into the G-layer toward the S2, preferentially in the CCs. Also in the small cells, corresponding to ends of the long wood fibers, an accumulation of aromatic substances at the CC is visible

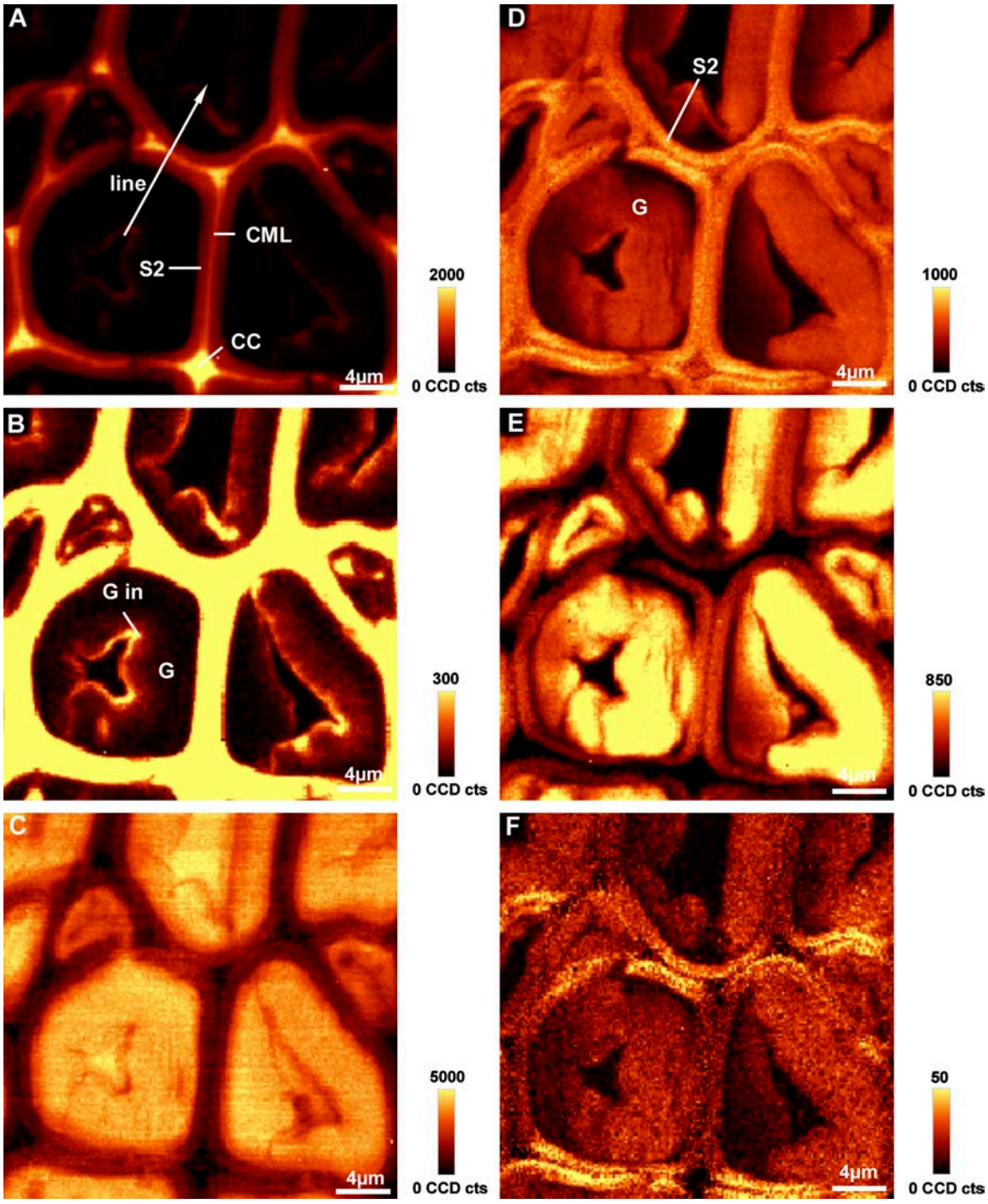

Figure 3. A to F, Raman images (30 × 30 μm) of poplar tension wood integrating over defined wavenumber areas. A, Intensity of the aromatic lignin band (1,550–1,640 cm^{-1}; marked line is analyzed in detail in Fig. 4). B, Intensity from 1,550 to 1,640 cm^{-1} with a changed intensity scaling to show lignin distribution within the G-layer. C, Intensity from 3,050 to 3,640 cm^{-1} (water). D, CC and C–O str. (carbohydrate region) from 1,026 to 1,195 cm^{-1}. E, C–H str. of cellulose (2,810–2,936 cm^{-1}). F, Intensity of the 1,097 cm^{-1} band (1,090–1,105 cm^{-1}).

(Fig. 3B). Plotting the intensity of the lignin band across the cell wall layers (line marked in Fig. 3A) shows that the lignin content diminishes almost to zero within the G-layer, but increases remarkably toward the lumen (Fig. 4A). The spectra taken from different positions (average spectra of the marked positions in Fig. 4A) across the cell wall clearly confirm the assumption that there are almost no aromatic substances in the G-layer, except in the inner lumen-side part. The aryl str. peak at 1,600 cm^{-1} is very small

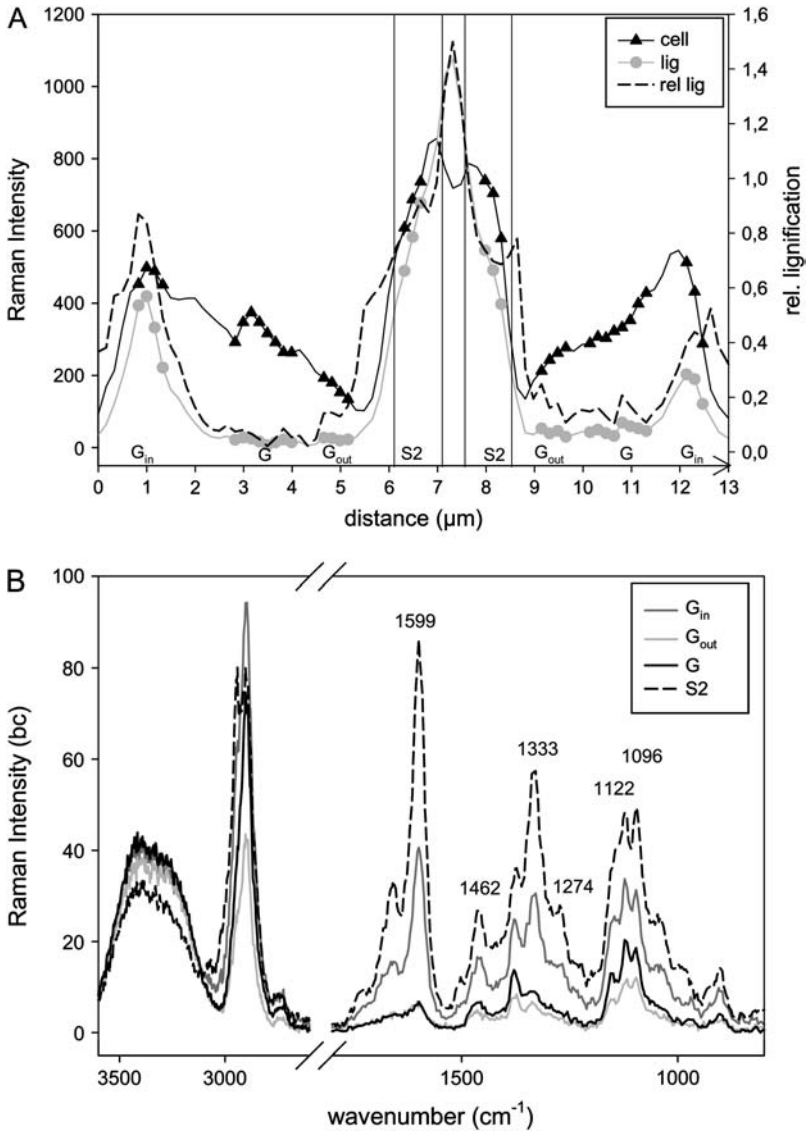

Figure 4. A and B, Intensity distribution of lignin (1,550–1,650 cm^{-1}), cellulose (cell: 1,026–1,195 cm^{-1}), and relative lignification (ratio of lignin to cellulose intensity) across the cell wall (line marked in Fig. 3A) of poplar G-fibers (A) and the corresponding bc spectra from the marked positions within the G (G, G_{in}, and G_{out}) and S2 layers (B).

in the middle (G) and outer part (G_{out}) and about half of the height in the inner part (G_{in}) compared to the S2 layer (Fig. 4B). This peak goes hand in hand with related bands at 1,462, 1,333, 1,274, and at 2,944 cm^{-1} (Fig. 4B). Positions and relative heights of the lignin related bands are very similar for the spectra of the S2 and inner G-layer, concluding that it is lignin and no other aromatic structures observed in this inner G-layer.

The occurrence of lignin in the G-layer during tension wood formation has long been debated (Pilate et al., 2004a). Some studies concluded that the G-layer mostly consists of cellulose and is totally free of lignin (Blanchette et al., 1994; Wada et al., 1995; Donaldson, 2001), whereas others found evidence for lignin (Yoshida et al., 2002; Joseleau et al., 2004). In this study, within the main part of the G-layer, lignin bands were weak, thus pointing to very minor amounts of lignin (Fig. 4, A and B). In the fiber ends (small cells), higher amounts were found as well as a thin (about 0.5 μm thick) more-lignified border toward the lumen (Figs. 3B and 4, A and B). Such an additional thin lignified layer could impede the degradation of the cellulosic G-layer and thus may act as a defense line against microorganisms.

The intensity in the OH region, showing the water distribution, is very high in the G-layer compared to the other more lignified cell wall layers (Fig. 3C). However, again toward the lumen, an inner small layer of more hydrophobic nature is seen (Fig. 3C). By integrating over the cellulose bands (1,026 to 1,195 cm^{-1}), the S2 layer is emphasized and the G-layer shows less intensity (Fig. 3D). Especially toward the S2 layer in some regions, less intensity is observed and the G-layer seems detached. A detailed look on the cellulose intensity across the line (marked in Fig. 3A) shows a gradual decrease within the G-layer on both sides toward the S2, an increase in the S2, and then again a decrease in the CML (Fig. 4A). These low cellulose intensity regions (Fig. 3D) are found in regions with higher intensity in the OH region (Fig. 3C) and may be

caused by uncontrolled swelling of the G-layer during cutting and, thus, changes in the focal plane. The G-layer in the investigated region is not a uniform layer tightly attached to the S2. Clair et al. (2005) suggested that the G-layer in tension wood is detached by cutting the transverse face of the wood block and can be blocked by embedding. But dehydrating and embedding the samples changes the natural state of the G-layer and thus, in this first approach, cutting and investigating without embedding was chosen.

The bands of the glycosidic linkage str. of the cellulose at 1,120 cm^{-1} (sym.) and 1,096 cm^{-1} (asym.) show less intensity within the G-layer compared to the S2 layer. The band at 2,897 cm^{-1} is sharp and high in the G-layer and no longer accompanied by the lignin-assigned band at 2,945 cm^{-1} (Fig. 4B). Integrating over the 2,897 cm^{-1} band enables accentuation of the G-layer compared to the S2 layer (Fig. 3E). The detachment in some regions is again seen by lower intensity. Analogous to the latewood case discussed in the previous section, imaging the intensity distribution of the 1,096 cm^{-1} band emphasizes (Fig. 1D) only cell wall layers in the direction of the electronic vector in x-direction of the image (Figs. 1D and 3F). We see that the S2 layer is emphasized in x-direction of the image, but no S1 layer can be distinguished. This can result either from cellulose orientation in the S2 similar to the S1 (high microfibril angle) and/or a small S2 and wide S1 layer, which contributes much to the signal. In this context, we note that tension wood fibers have been observed to show high structural variability in the cell wall organization with different layer combinations: S1-S2-G, S1-S2-S3-G, and S1-G (Dadswell and Wardrop, 1955).

In the S2 layer the 1,096 cm^{-1} band is as high as the 1,122 cm^{-1} band, while in the G-layer a smaller 1,096 cm^{-1} band is observed (Fig. 4B). Assisted by the changes in the intensity of the 2,897 cm^{-1} band, we can infer different cellulose orientations for the G-layer and adjacent S2 layer. In the G-layer, cellulose molecules lie parallel to the fibers (perpendicular to the sample plane), whereas in the S2 the cellulose is less perpendicular to the plane. Independent observations have shown that the cellulose in the G-layer of tension wood is highly crystalline and parallel oriented (Dadswell and Wardrop, 1955; Pilate et al., 2004b). Additional characteristics of the G-layer spectra are the disappearance of the shoulder around 1,143 cm^{-1} and the band at 1,045 cm^{-1} (Fig. 4B). These two bands, also found in the G-layer adjacent to the lumen where lignin was detected (G_{in}), cannot be clearly assigned at the moment, but seem to be associated with lignin (Table I).

Advantages and Limitations

Raman imaging allowed separating small cell wall layers, such as the S1 in latewood (Fig. 1D) and a 0.5 μm thick lignified layer in tension wood (Fig. 3B). Marking and averaging spectra enabled us to get more detailed information from these small distinct regions. Without Raman imaging it would be difficult to localize the laser spot exactly on such a small layer of interest. Furthermore, Raman imaging allows very short integration times (1 s) to avoid sample degradation. However, contributions from the adjacent layer might be noticed when deriving average spectra of small layers (e.g. CML, S1). Indeed, though the theoretical diffraction-limited laser spot size is 0.32 μm, the actual size will be larger due to effects of residual aberrations and objective manufacturing tolerances.

Because of the multicomponent nature of wood, its vibrational spectrum is rather complex with broad overlapping bands. Cellulose and hemicelluloses have similar chemical bonds and are therefore difficult to discern (Agarwal and Ralph, 1997). Generally, the skeletal motions of most of the hemicelluloses will result in fairly broad bands, unless they are so organized that they have a high degree of repetitive order. Therefore, it was not possible to draw conclusions regarding the hemicelluloses. In contrast, the cellulose bands are rather sharp and influenced by orientation and crystallinity and changes in cellulose orientation have to be taken into account when following spatial variation of cellulose band intensities. Orientation effects could be better quantified if the same location could be analyzed with the electric vector direction of the laser beam rotated.

Lignin distribution has been studied in the xylem of gymnosperms and angiosperms using a variety of techniques, such as UV microscopy (e.g. Koch and Kleist, 2001), energy dispersive x-ray analysis (e.g. Westermark et al., 1988), and interference and fluorescence microscopy (e.g. Donaldson et al., 2001). By Raman microscopy, lignin was shown to be oriented in the plant cell wall (Atalla and Agarwal, 1985). The strong aromatic contribution around 1,600 cm^{-1} enabled the imaging of the lignin distribution by integrating over this wavenumber area (Figs. 1A and 3, A and B). In our imaging studies no orientation effects were observed for lignin and we believe that this is because any (small) orientational changes of the lignin are lost in the much larger changes in lignin intensity observed between different layers.

In summary, the major assets of Raman microscopy are that samples can be investigated in situ without any embedding, staining, or chemical pretreatment and that information regarding the lignin and cellulose content and their orientation in wood may be gained at the same time. However, for a more detailed understanding of both, a wider array of samples as well as combination of results from Raman with other established techniques (e.g. UV microscopy) are necessary.

CONCLUSION

In short, our results clearly illustrate the application of scanning Raman microscopy to nondestructive in situ chemical imaging of plant cell walls. Differences

in cell wall polymer composition between and within the cell wall layers have been imaged with high spatial resolution. In addition, the technique also enables detection of changes in orientation of the cellulose molecules. Nevertheless, to extract all the information lying in the spectra behind the chemical mapping, more detailed knowledge on bands and the influence of composition and orientation changes has to be gained. Investigation of a wider range of cell wall variants, including chemically modified systems, will help us to gain better knowledge of plant cell wall structure and organization.

MATERIALS AND METHODS

Samples were taken in autumn from a 2-year-old hybrid poplar (*Populus nigra* × *Populus deltoids* i14551, artificial tilt). Without any further sample preparation, 20-μm-thick sections were cut on a rotary microtome (LEICA RM2255), immediately placed on a glass slide with a drop of water, and sealed with a coverslip to avoid evaporation of water during the measurement. The shown examples derive from one cross section, sampled once in the latewood near the cambium and again in a tension wood zone built in the spring before.

Spectra were acquired with a confocal Raman microscope (CRM200, WITEC) equipped with a piezo scanner (P-500, Physik Instrumente) and a high numerical aperture (NA) microscope objective from Nikon (100 oil NA = 1.25). A linear polarized laser (diode pumped green laser, λ = 532 nm, CrystaLaser) was focused with a diffraction-limited spot size (0.61 λ/NA) and the Raman light was detected by an air-cooled, back-illuminated spectroscopic CCD (ANDOR) behind a grating (600 g mm^{-1}) spectrograph (ACTON) with a resolution of 6 cm^{-1}. The laser power on the sample was approximately 5 mW. For mapping an integration time of 1 s and 0.17 μm, steps were chosen and every pixel corresponds to one scan.

The ScanCtrlSpectroscopyPlus software (WITEC) was used for measurement setup and image processing. Chemical images were achieved by using a sum filter, integrating over defined wavenumber areas in the wood spectrum. The filter calculates the intensities within the chosen borders and the background is subtracted by taking the baseline from the first to the second border. The overview chemical images (Figs. 1 and 3) enabled us to separate cell wall layers and to mark defined distinct cell wall areas to calculate average spectra from these areas of interest (Fig. 2). As the cell wall sublayers have different area fractions, the number of spectra used for calculation of average spectra for each sublayer varied. For a detailed analysis of the intensity and the shape of the spectra along the cell wall layers in tension wood, a line was drawn across the tension wood cell wall (Fig. 3A). Band intensity and spectra were analyzed along this line (Fig. 4, A and B). To achieve good quality spectra, three or four spectra were averaged from the left and right side of the line.

The calculated average spectra were baseline corrected and analyzed with the OPUS software package (version 4.2). Bands assigned according to the literature (Wiley and Atalla, 1987; Agarwal and Ralph, 1997; Agarwal, 1999) are summarized in Table I.

ACKNOWLEDGMENTS

Jong Seto and Dr. Himadri S. Gupta (Max-Planck-Institute of Colloids and Interfaces, Potsdam) are acknowledged for the linguistic revision of the manuscript. Many thanks to Dr. Catherine Coutand (Institut National de la Recherche Agronomique, Clermont Ferrant) for the gift of the poplar sample.

Received June 14, 2005; revised January 12, 2006; accepted January 29, 2006; published February 17, 2006.

LITERATURE CITED

Agarwal UP (1999) An overview of Raman spectroscopy as applied to lignocellulosic materials. *In* DS Argyropoulos, ed, Advances in Lignocellulosics Characterization. TAPPI Press, Atlanta, pp 209–225

Agarwal UP, Atalla RH (1986) In-situ Raman microprobe studies of plant cell walls: Macromolecular organization and compositional variability in the secondary wall of *Picea mariana* (Mill.) B.S.P. Planta **169:** 325–332

Agarwal UP, Ralph S (1997) FT-Raman spectroscopy of wood: identifying contributions of lignin and carbohydrate polymers in the spectrum of black spruce (*Picea mariana*). Appl Spectrosc **51:** 1648–1655

Atalla RH, Agarwal UP (1985) Raman microprobe evidence for lignin orientation in the cell walls of native woody tissue. Science **227:** 636–638

Bamber R (2001) A general theory for the origin of growth stresses in reaction wood: how trees stay upright. IAWA J **22:** 205–212

Barnett JR, Bonham VA (2004) Cellulose microfibril angle in the cell wall of wood fibers. Biol Rev Camb Philos Soc **79:** 461–472

Barnett JR, Jeronimidis G (2003) Reaction wood. *In* JR Barnett, G Jeronimidis, eds, Wood Quality and Its Biological Basis. Blackwell Scientific Publisher, Oxford, p 226

Blanchette RA, Obst JR, Timell TE (1994) Biodegradation of compression wood and tension wood by white and brown rot fungi. Holzforschung **48:** 34–42

Chenery D, Bowring H (2003) Infrared and Raman spectroscopic imaging in bioscience. Spectroscopy Europe **15:** 8–14

Clair B, Thibaut B, Sugiyama J (2005) On the detachment of the gelatinous layer in tension wood fiber. J Wood Sci **51:** 218–221

Côté WA Jr, Day AC (1965) Anatomy and ultrastructure of reaction wood. *In* WA Coté, ed, Cellular Ultrastructure of Woody Plants. Syracuse University Press, Syracuse, NY, pp 391–418

Côté WA Jr, Day AC, Timell TE (1969) A contribution of the ultrastructure of tension wood fibres. Wood Sci Technol **3:** 257–271

Dadswell HE, Wardrop AB (1955) The structure and properties of tension wood. Holzforschung **9:** 97–103

Donaldson L, Hague J, Snell R (2001) Lignin distribution in coppice poplar, linseed and wheat straw. Holzforschung **55:** 379–385

Donaldson LA (2001) Lignification and lignin topochemistry—an ultrastructural view. Phytochemistry **57:** 859–873

Edwards HGM, Farwell DW, Webster D (1997) FT Raman microscopy of untreated natural plant fibres. Spectrochim Acta [A] **53:** 2383–2392

Fengel D, Wegener G (1989) Wood: Chemistry, Ultrastructure, Reactions. Walter de Gruyter & Co., Berlin

Himmelsbach DS, Khahili S, Akin DE (1999) Near-infrared–Fourier-transform–Raman microspectroscopic imaging of flax stems. Vib Spectrosc **19:** 361–367

Joseleau JP, Imai T, Kuroda K, Ruel K (2004) Detection in situ and characterization of lignin in the G-layer of tension wood fibres of Populus deltoides. Planta **219:** 338–345

Jourez B, Riboux A, Leclercq A (2001) Anatomical characteristics of tension wood and opposite wood in young inclined stems of poplar (*Populus euramericana* CV ''Ghoy''). IAWA J **22:** 133–157

Kacuráková M, Capeka P, Sasinková V, Wellner N, Ebringerova A (2000) FT-IR study of plant cell wall model compounds: pectic polysaccharides and hemicelluloses. Carbohydr Polym **43:** 195–203

Koch G, Kleist G (2001) Application of scanning UV microspectrophotometry to localise lignins and phenolic extractives in plant cell walls. Holzforschung **55:** 563–567

McCann MC, Bush M, Milionia D, Sadoa P, Stacey NJ, Catchpole G, Defernez M, Carpita NC, Hoft H, Ulvskov P, et al (2001) Approaches to understanding the functional architecture of the plant cell wall. Phytochemistry **57:** 811–821

McCann MC, Hammouri M, Wilson RH, Belton P, Roberts K (1992) Fourier transform infrared microspectroscopy is a new way to look at plant cell walls. Plant Physiol **100:** 1940–1947

Mellerowicz EJ, Baucher M, Sundberg B, Boerjan W (2001) Unravelling cell wall formation in the woody dicot stem. Plant Mol Biol **47:** 239–274

Morris VJ, Ring SG, MacDougall AJ, Wilson RH (2003) Biophysical characterisation of plant cell walls. *In* J Rose, ed, The Plant Cell Wall—Annual Plant Reviews. Blackwell Publishing, Oxford, pp 55–91

Pilate G, Chabbert B, Cathala B, Yoshinaga A, Leplé JC, Laurans F, Lapierre C, Ruel K (2004a) Lignification and tension wood. C R Biol **327:** 889–901

Pilate G, Déjardin A, Laurans F, Leplé J-C (2004b) Tension wood as a model for functional genomics of wood formation. New Phytol **164:** 63–72

Plomion C, Leprovost G, Stokes A (2001) Wood formation in trees. Plant Physiol **127:** 1513–1523

Rösch P, Schneider H, Zimmermann U, Kiefer W, Popp J (2004) In situ Raman investigation of single lipid droplets in the water-conducting xylem of four woody plant species. Biopolymers **74:** 151–156

Saariaho AM, Jääskeläinen AS, Nuopponen M, Vuorinen T (2003) Ultra violet resonance Raman spectroscopy in lignin analysis: determination of characteristic vibrations of p-hydroxyphenyl, guaiacyl, and syringyl lignin structures. Appl Spectrosc **57:** 58–66

Salzer R, Steiner G, Mantsch HH, Mansfield J, Lewis EN (2000) Infrared and Raman imaging of biological and biomimetic samples. Fresenius J Anal Chem **366:** 712–726

Sauter JJ, van Cleve B (1994) Storage, mobilization and interrelations of starch, sugars, protein and fat in the ray storage tissue of poplar trees. Trees (Berl) **8:** 297–304

Schrader B (1995) Infrared and Raman Spectroscopy: Methods and Applications. VCH, Weinheim, Germany

Séné CFB, McCann MC, Wilson RH, Crinter R (1994) Fourier-transform Raman and Fourier-transform infrared spectroscopy: an investigation of five higher plant cell walls and their components. Plant Physiol **106:** 1623–1631

Smith E, Dent G (2005) Modern Raman Spectroscopy: A Practical Approach. John Wiley & Sons, Chicester, England

Stewart D (1996) Fourier transform infrared microspectroscopy of plant tissues. Appl Spectrosc **50:** 357–365

Sugiyama K, Okuyama T, Yamamoto H, Yoshida M (1993) Generation process of growth stresses on cell walls: relation between longitudinal released strain and chemical composition. Wood Sci Technol **27:** 257–262

Timell TE (1969) The chemical composition of tension wood. Sven Papperstidn **6:** 173–181

Toole GA, Kacuráková M, Smith AC, Waldron KW, Wilson RH (2004) FT-IR study of the *Chara corallina* cell wall under deformation. Carbohydr Res **339:** 629–635

Wada M, Okano T, Sugiyama J, Horii F (1995) Characterization of tension and normally lignified wood cellulose in *Populus maximowiczii.* Cellulose **2:** 223–233

Westermark U, Lidbrandt O, Eriksson I (1988) Lignin distribution in spruce (*Picea abies*) determined by mercurization with SEM-EDXA technique. Wood Sci Technol **22:** 243–250

Wiley JH, Atalla RH (1987) Band assignment in the raman spectra of celluloses. Carbohydr Res **160:** 113–129

Yamamoto H (1998) Generation mechanism of growth stresses in wood cell walls: roles of lignin deposition and cellulose microfibril during cell wall maturation. Wood Sci Technol **32:** 171–182

Yoshida M, Ohta H, Yamamoto H, Okuyama T (2002) Tensile growth stress and lignin distribution in the cell walls of yellow poplar, *Liriodendron tulipifera* Linn. Trees (Berl) **16:** 457–464